Talanta 118 (2014) 382–388

Contents lists available at ScienceDirect

Talanta

journal homepage: www.elsevier.com/locate/talanta

Metabonomic study on the antitumor effect of flavonoid derivative 3d in HepG2 cells and its action mechanism

Dan Gao [a,b,1], Feng Jin [a,c,1], Hongxia Liu [b,*], Yini Wang [b], Yuyang Jiang [a,d,*]

[a] State Key Laboratory Breeding Base-Shenzhen Key Laboratory of Chemical Biology, Graduate School at Shenzhen, Tsinghua University, Shenzhen 518055, China
[b] Key Laboratory of Metabolomics at Shenzhen, Shenzhen 518055, China
[c] Neptunus Pharmaceutical Technology Center, Shenzhen 518057, China
[d] School of Medicine, Tsinghua University, Beijing 100084, China

ARTICLE INFO

Article history:
Received 17 June 2013
Received in revised form
10 September 2013
Accepted 16 September 2013
Available online 25 September 2013

Keywords:
Metabolomics
UPLC/Q-TOF MS
Flavonid derivate
HepG2 cells
Action mechanism

ABSTRACT

A novel flavonid derivate, 1-(3-chloro-4-(6-ethyl-4-oxo-4H-chromen-2-yl)phenyl)-3-(4-chlorophenyl) urea (3d) synthesized in our lab possesses potent antitumor activity against HepG2 cells. Our previous studies on pharmacological mechanism of 3d mostly focused on cell and gene levels, little is about its metabolomics study. Herein, an ultra-performance liquid chromatography coupled to quadrupole time-of-flight mass spectrometry (UPLC/Q-TOF MS) based metabolomics approach was established to investigate the antitumor effect of 3d on HepG2 cells and its action mechanism. Q-TOF MS was used to identify metabolites, and tandem mass spectrometry was used to confirm their identity. Comparing 3d-treated HepG2 cells with vehicle control (dimethyl sulfoxide), 32 distinct metabolites involved in glutathione metabolism, glycerophospholipid metabolism, cysteine and methionine metabolism, fatty acid metabolism, and phenylalanine metabolism. The reduced level of glutathione (GSH) and decreased ratio of reduced/oxidized glutathione (GSH/GSSG) in 3d-treated cells indicated the increased oxidative stress after 3d treatment. The significant decrease of phosphatidylcholine (PC) levels and increase of lysophosphatidylcholine (LPC) levels suggested alterations in lipid composition which were causally related to decline in mitochondrial function. Depletion of carnitine and increase of long chain carnitines and fatty acids reflected decline in fatty acid metabolism. The further biological experiments including ROS and MMP measurements confirmed the above probabilities presumed from metabolomic results. Our findings suggested that 3d caused the perturbation of multiple cellular pathways. The increased oxidative stress and the resulting mitochondrial dysfunction resulted in the antiproliferative effect of 3d. The UPLC/Q-TOF MS based metabolomics approach provides new insights into the mechanistic studies of new compounds that distinct from traditional biological studies.

1. Introduction

Flavonoids are widely distributed natural products in plants which include flavones, flavonols, iso-flavones, chalcones, etc. [1]. Flavonoids present extensive range of biological effects and pharmacological activities, such as antitumor, anti-inflammatory, antiviral, and cardio-protective properties [2,3], and most of these biological activities are often associated with their antioxidant activity [4]. Among these properties, the antitumor activity has attracted an increasing interest in the development of flavonoids and their derivatives as new drugs. A large number of studies have demonstrated that flavoniods conducting as potential antitumor agents are based on the mechanisms including induction of apoptosis, cell cycle arrest, modulation of protein kinase activities, and the modification of signal transduction pathways on cancer cells [5–8]. Up to now, the understanding of their antitumor mechanisms mostly focuses on cell and gene levels. However, there is little known about their metabolomic study. The analysis of metabolic profiling of cells underlying drug treatment will greatly facilitate the understanding on drug-cell interactions.

Metabolomics is a quantitative approach to study the entire pattern of low molecular weight compounds, widely used to analyze microorganisms in the past [9]. Moreover, the variations of metabolite concentrations display the changes in genomics and proteomics and responses of cells and tissues to external stimuli [10–12]. Recently, metabolomics has become a powerful tool for disease diagnosis and monitoring [13], assessing therapeutic and toxic effects of many drugs [14,15], and food safety research [16]. There are a number of methodologies used for metabolomic

* Corresponding authors. Tel./fax: +86 755 2603 6035.
E-mail addresses: liuhx@sz.tsinghua.edu.cn (H. Liu), jiangyy@sz.tsinghua.edu.cn (Y. Jiang).
[1] Dan Gao and Feng Jin contributed equally to this work.

0039-9140/$ - see front matter © 2013 Elsevier B.V. All rights reserved.
http://dx.doi.org/10.1016/j.talanta.2013.09.018

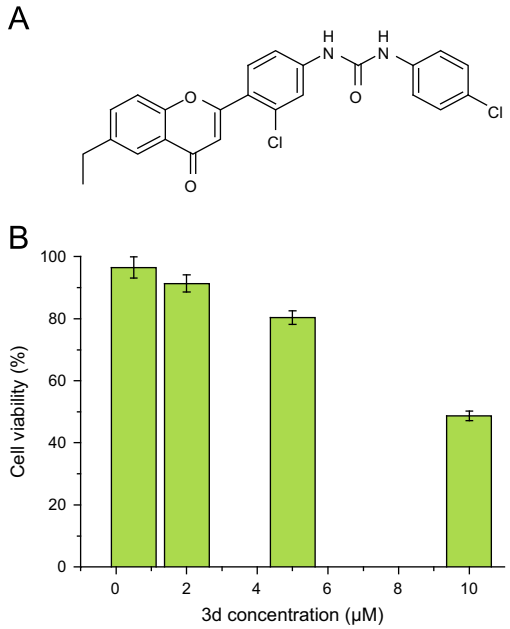

Fig. 1. (A) Chemical structure of flavonoid derivative 3d. (B) The cytotoxicity of 3d at different concentrations on HepG2 cells after 24 h incubation using the MTT assay.

including nuclear magnetic resonance (NMR) spectroscopy [17], gas chromatography–mass spectrometry (GC–MS) [18], liquid chromatography–mass spectrometry (LC–MS) [19,20], and capillary electrophoresis–mass spectrometry (CE–MS) [21]. Compared to LC–MS, UPLC–MS possessing several advantages is more appropriate for metabolomics research, such as better chromatographic peak resolution, shorter analysis time and higher sensitivity.

In our previous work, a flavonoid derivative, 1-(3-chloro-4-(6-ethyl-4-oxo-4H-chromen-2-yl)phenyl)-3-(4-chlorophenyl)urea (3d) (Fig. 1A) was synthesized, which possessed potent antitumor activity against HepG2 cells, while lower toxicity against normal liver cell-lines (QSG7701 and HL7702). The antitumor mechanism had been explored by conventional molecular biological methods including flow cytometry, western blot, and *in vitro* kinase assays. However, the effect of 3d on metabolic profiling is still lacking. The information is vital to a thorough understanding of the antiproliferation action of 3d. In this work, metabolomics study based on ultra-performance liquid chromatography coupled to quadrupole time-of-flight mass spectrometry (UPLC/Q-TOF MS) was established to investigate the metabolic profiling of HepG2 cells induced by 3d to explore its probable antitumor mechanism. Distinct biomarkers caused by 3d were identified and their metabolic pathways were also discussed. Furthermore, the biological events were validated by conventional molecular biology. Our results suggested that 3d caused mitochondrial malfunction and disturbances in the metabolic pathway and network, and eventually resulted in celluar antiproliferation.

2. Experimental section

2.1. Reagents and materials

3d was synthesized by our lab. Acetonitrile and methanol (HPLC grade) were purchased from Fisher (Fairlawn, USA). HPLC grade formic acid was purchased from Tedia (Tedia Co., USA). Dulbecco's Modified Eagle's Media (DMEM) and fetal bovine serum (FBS) were purchased from Gibco Corporation (Grand Island, NY). Water was purified by redistillation and filtered through 0.22 μm membrane filter before use. Reactive oxygen species assay kit and Rhodamine 123 (Rh123) were purchased from Beyotime Institute of Biotechnology (Shanghai, China).

2.2. Cell viability assay

HepG2 cells were cultured in DMEM containing 10% FBS, 100 μg/mL penicillin, and 100 μg/mL streptomycin. Cells were kept at 37 °C in 5% CO_2-humidified air atmosphere with the medium replaced every 24 h. For cell viability assay, HepG2 cells were harvested and seeded in 96-well plates at the concentration of 5000 cells per well. An initial stock solution of 10 mM 3d was prepared in dimethyl sulfoxide (DMSO). 3d solutions were serial diluted in DMEM to obtain final concentrations ranging from 0.5 to 10 μM, and then incubated with HepG2 cells at 37 °C in a 5% CO_2 incubator for 24 h. Medium containing the same concentration of DMSO was used as a vehicle control. 10 μL of MTT solution (5 mg/mL in PBS) was then added to each well and incubated for 4 h at 37 °C. 100 μL DMSO was added to dissolve the formazan precipitate and the absorbance at 495 nm was determined using Multimode Detector DTX880 (Beckman Coulter).

2.3. Sample preparation

1×10^7 cells were exposed to 5 μM of 3d with equal amounts of DMSO as controls. Eight replicates for each group were analyzed. The final concentration of DMSO was less than 0.1%. After 24 h incubation, the culture medium was removed from the culture dish, cells were quickly washed by gently dispensing 10 mL of 37 °C deionized water to the cellular surfaces [22]. The plate was rocked briefly within 2 s, aspirated, and quenched by directly adding 1 mL of cold methanol/water (4:1). For extraction, plates were immediately transferred to an ice bath and 1 mL of ice cold 80% aqueous methanol was added to each plate and cells were scraped/suspended with a cell lifter. The cell pellets were transferred to 2.5 mL micro-centrifuge tubes, ultrasonicated in an ice bath ultra-sonicator for 10 min, and subsequently centrifuged at 4 °C for 3 min at 16,000 g. Supernatants were collected and dried with a stream of nitrogen. The residues were resuspended in 1 mL of acetonitrile/water (1:1, v/v) mixture, and were filtered through 0.22 μm mesh Millipore filters into glass auto-samplers. The samples were stored at −80 °C prior to analysis. In parallel a quality control (QC) sample was prepared by mixing equal volumes of 30 μL into a glass auto-sampler from each of the 16 samples. The pooled QC sample was injected five times at the beginning of the run in order to ensure system equilibration and then every five samples to further monitor the stability of the analysis.

2.4. UPLC/Q-TOF MS conditions

Analyses were performed using Acquity™ Ultra-Performance Liquid Chromatography system coupled to Q-TOF Premier Mass Spectrometer (Waters Corporation, MA, USA), operated in the positive (ESI+) and negative (ESI-) electrospray ionization modes. Chromatrographic separation was carried out at 35 °C on a Waters Acquity™ BEH C18 (1.7 μm, 2.1 mm × 100 mm) with the following solvent system: A=0.1% formic acid in water, B=acetonitrile in positive ion mode; A1=5 mM ammonium acetate in water and B1=acetonitrile in negative ion mode. Elution gradient was linearly increased from 5% to 40% B (B1) within 4 min, then to 100% B (B1) within 5 min and held for 1 min, followed by return to 5% B (B1). Total running time was 14 min per separation. The injection volume was 10 μL. ESI conditions were source temperature 120 °C, desolvation temperature 300 °C, cone gas flow 50 L/h, desolvation gas flow 550 L/h, capillary voltage for ESI+ 3.0 kV, for ESI- 2.5 kV, cone voltage 30 V. The instrument was calibrated before analyses using 0.5 mM sodium formate solution. The mass spectral

results were obtained under the *m/z* range 50–1000 with scan time of 0.2 s and an interscan delay of 0.02 s. Data were collected in centroid mode. Leucine Enkephalin (MW=555.62 Da) (100 pg/μL in acetonitrile/water 50:50) was used as a lock mass with a flow rate of 0.05 mL/min. Lock spray frequency was set at 10 s, and the lock mass data were averaged over 10 s for correction. The reference cone voltage was set at 30 V. For MS/MS analysis, collision energies were set in ramp mode ranged from 10 V to 30 V.

2.5. Data processing and multivariate statistical analysis

The raw data from the spectral analysis of cellular extracts was processed using Micromass MarkerLynx Applications Manager version 4.1 (Waters Corporation, MA, USA) [23]. The analyzed spectral data was transformed into a single matrix containing aligned peaks with the same mass/retention time (RT) pair along with normalized peak intensities and sample name. The major parameters for data processing were set as follows: retention time (0–10 min), mass range (50–1000 Da), mass tolerance (0.05 Da), intensity threshold (10 counts), maximum mass per retention time (6) and retention time tolerance (0.2 min). Prior to multivariate statistical analysis, the noise and background interference was excluded, and the total sum of the chromatogram was normalized [24]. The resulting data set was then introduced into SIMCA-P 11.5 software package (Umetrics, Umea, Sweden), and the data was mean-centered and pareto-scaled prior to multivariate statistical analysis. Unsupervised principle component analysis (PCA) was initially used to detect intrinsic clustering and obvious outliers between 3d-treated group and control group. In order to visualize the maximal difference of global metabolic profiles within the sample set, partial least squares discriminant analysis (PLS-DA) was further carried out.

All data represent at least three independent experiments and are expressed as means ± standard deviation (SD). Statistical significance was determined using a non-corrected two-tailed Student's *t*–test, unpaired assuming equal variance. A *p*-value of < 0.05 was considered significant. Databases of HMDB (http://www.hmdb.ca/) and METLIN (http://metlin.scripps.edu/) were used to identify the metabolic markers with tandem mass spectrometry (MS/MS). Standards of metabolic interest were used to confirm their structures.

2.6. Detection of reactive oxygen species (ROS) and mitochondrial transmembrane potential (MMP)

The levels of intracellular ROS and MMP were determined according to their described protocols respectively. Cells were treated with 0, 5, 10, and 20 μM of 3d for 24 h, harvested, and resuspended in PBS. Cells were then incubated separately with 10 μM 2′,7-dichlorfluorescein-diacetate (DCFH-DA) and 2 μM Rh123 in dark for 30 min at 37 °C for ROS and MMP detection. The fluorescence was detected with a fluorescence spectrophotometer (ROS, Ex=485 nm and Em=525 nm; MMP, Ex=507 nm and Em=529 nm).

3. Results and discussion

3.1. Antiproliferative action of 3d

Prior to metabolomics study, the effect of 3d concentration on HepG2 cell viability was investigated to acquire the optimal drug effect together with minimal cell death. As shown in Fig. 1B, with the increasing concentration of 3d, cell viability decreased unobviously when the concentrations were less than 5 μM. However, when the concentration increased to 10 μM, only about 50% cells were viable. When 3d concentration was 5 μM, the viability of HepG2 cells was approximately 80% which was appropriate for metabolomics study. Therefore, 5 μM of 3d was applied for the following experiments.

3.2. Multivariate statistical analysis and identification of intercellular discriminate metabolites

In order to investigate the metabolic fingerprints in HepG2 cells, the metabolites in vehicle control and 3d-treated cells were profiled by UPLC/Q-TOF MS in both positive and negative modes. However, the positive ion mode gave more information rich date than negative ion mode. Respective base peak intensity (BPI) chromatograms are shown in Fig. 2. Raw data from UPLC/Q-TOF MS were analyzed by the MarkerLynx software. RT, m/z, and peak height intensities were imported into SIMCA-P software for data analysis. PCA and PLS-DA are the two most popular pattern recognition methods to get information for classification and to identify metabolites [25–27]. PCA, an unsupervised multivariate statistical method, is applied as the first step in the separation procedure to identify significant clusters in an unsupervised manner. PLS-DA, a supervised method, possessing the similar principle with PCA, is used to enhance the classification performance [28]. In our study, multivariate data analysis was performed using the PCA method. Two principal components were created by the SIMCA-P software. Fig. 3A shows the PCA score plot representing the distribution between the control and 3d-treated HepG2 cell groups in two dimensions. The obvious separation between the two groups indicated that intercellular metabolites have obvious perturbation under the treatment of 3d. The corresponding loading plot used to identify biomarkers is shown in Fig. 3B. The ions furthest away from the origin contribute significantly to the clustering of the two groups and may be regarded as the potential biomarkers. In addition, the QC data was used to investigate the analytical variability in the whole run, which was critical for evaluating the variation in the analytical results and the reliability of the metabolite profiling data [29]. As shown in Fig. 3A, the QC samples were tightly clustered together in the PCA score plot which indicated that the inter-sample repeatability was acceptable providing the confidence in the quality of the data.

An independent *t*-test was used to reveal the significant differences between the control and 3d-treated cell groups. The metabolites which have statistically significantly between the two groups after correction for multiple comparisons ($p < 0.05$) were identified. A total of 32 significant changed metabolites were identified in positive and negative ion modes. Metabolite identifications were performed with high resolution MS spectra and corresponding MS/MS fragments. Their fragmentation patterns were compared with those of the corresponding pure compounds in the database HMDB and METLIN. Some interested metabolite standards were confirmed by comparison of RT and isotopic distribution of commercially available reagents with those obtained in real samples. A list of metabolites except for those involved in glutathione metabolism, glycerophospholipid metabolism and fatty acid metabolism are summarized in Table 1, including RT, the mass obtained in UPLC–MS system, and the mass error when comparing with the database. In addition, the type of the identification (MS/MS fragmentation or confirmation with the analysis of standard), fragment ions of the metabolite, percentage of changes in different comparisons, and statistical significance were also presented in the table.

3.3. Metabolic pathway analysis

The metabolic pathway analysis with MetPA (www.metaboanalyst.ca) [30] revealed that the identified biomarkers involved in glutathione metabolism, cysteine and methionine metabolism, and glycerophospholipid metabolism were disturbed in 3d-treated

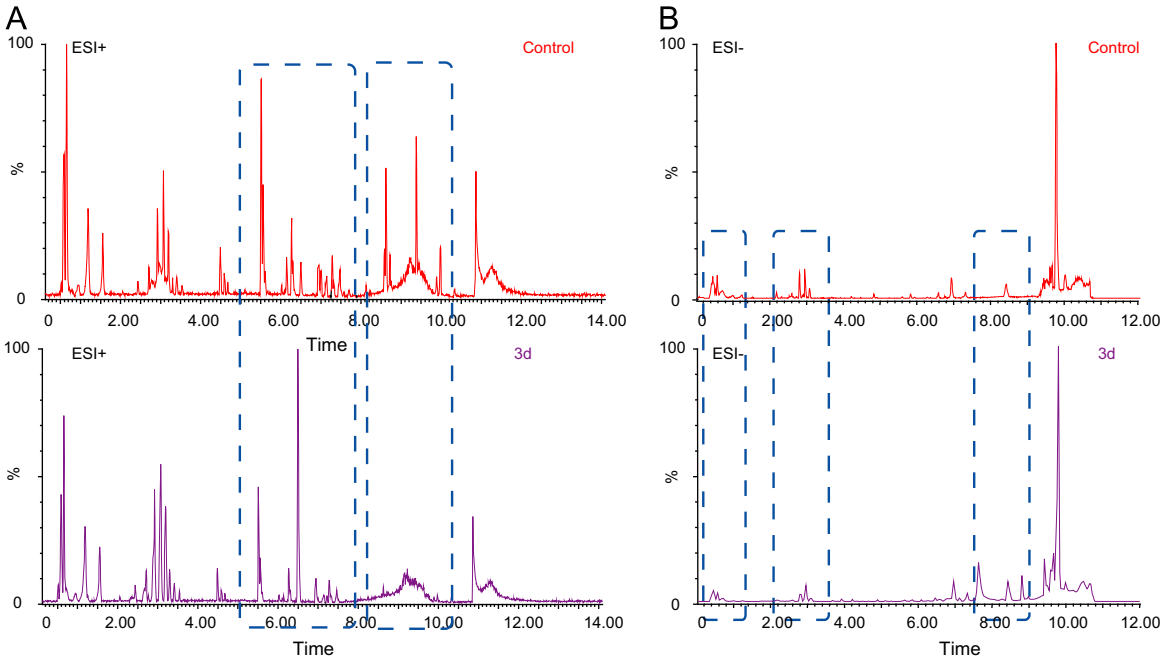

Fig. 2. BPI chromatograms obtained from HepG2 cell extracts with and without 3d treatment in positive (A) and negative (B) ion modes.

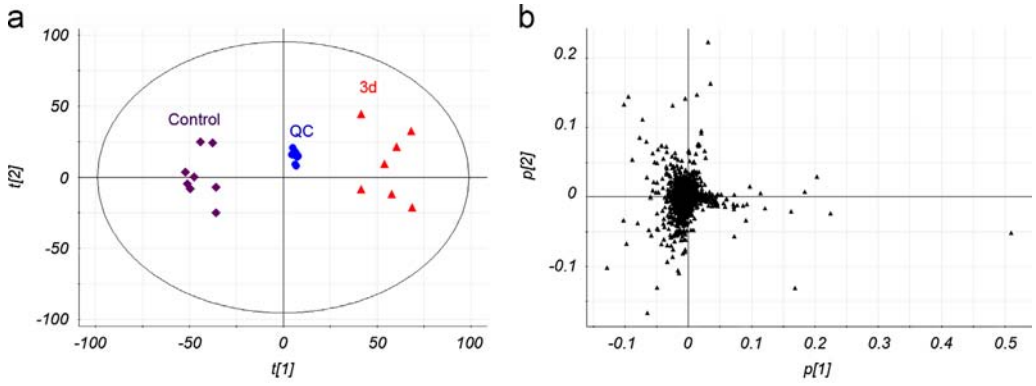

Fig. 3. Principal component analysis (PCA) of extracted metabolites in HepG2 cells with or without 3d treatment in positive ion mode. (A) PCA scores plot. Solvent control (◆), Quality control (●), and 3d treated group (▲) are included. (B) PCA loading plot.

Table 1
Identification of metabolites except for glutathione metabolism, glycerophospholipid metabolism and fatty acid metabolism.

Compound	RT (min)	Measured mass (Da)	Mass error (ppm)	Fragment ions	Fold changes [a](3d/control)
Hypoxanthine[d]	0.5415	137.0487	0.21	67.0997, 94.0379, 119.0392	0.82
Glu Leu[d]	0.5540	261.1494	0.19	86.0962, 130.0686, 148.0507	0.75
L-Phenylalanine[d]	0.5605	164.072	1.83	72.0255, 103.0768, 147.0599	0.34
L-tryptophan[d]	0.5517	205.1033	0.30	118.0691, 146.0577, 188.0782	0.48
Glu Glu Glu[d]	0.5687	406.1492	8.86	179.0491, 308.0896, 406.1492	0.65
S-Adenosylhomocysteine[d]	0.5528	385.1304	2.34	87.9608, 134.0586, 250.0627	1.24
Uridine[d]	0.5582	243.0609	5.76	82.0289, 110.0244, 200.0511	0.08
Guanosine[d]	0.5603	282.0872	−6.03	108.0217, 133.0098, 150.0452	0.36
Oxyquinoline[d]	1.4593	146.0607	4.79	91.0558, 101.0401, 118.0627	0.70
Stearic acid[d]	6.4511	283.2642	0.71	Standard	2.12
Palmitic acid[d]	6.8020	255.2288	16.10	Standard	1.85
LysoPE[b](18:1)[e]	7.4383	478.2954	3.14	196.0386, 281.2558, 417.3629	0.04
PG[c](18:1/22:5)[e]	9.4953	821.5376	4.63	255.2357, 281.2476, 766.5377	1.86
PG(18:1/18:1)[e]	9.9153	773.5332	1.81	152.9966, 255.2280, 281.2543,	7.16

[a] Fold change was calculated from the arithmetic mean values of each group.
[b] LysoPE: Lysophosphoethanolamine.
[c] PG: phosphatidylglycerol.
[d] Metabolites formally identified by standard samples.
[e] Metabolites putatively annotated.

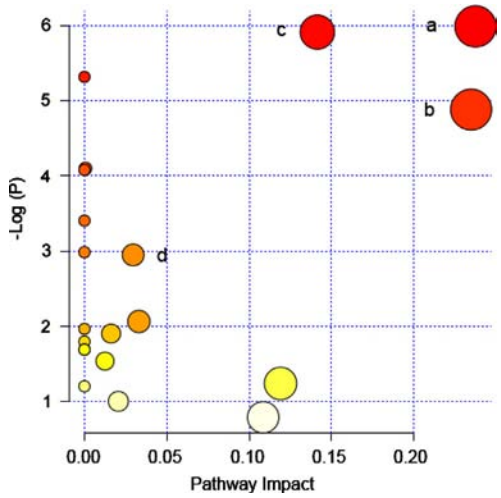

Fig. 4. (A) Summary of pathway analysis with MetPA. (a) glutathione metabolism; (b) cysteine and methionine metabolism, (c) glycerophospholipid metabolism, and (d) fatty acid metabolism.

group (Fig. 4). The impact values of glutathione metabolism, cysteine and methionine metabolism, and glycerophospholipid metabolism were 0.24, 0.23, and 0.14 respectively. The pathway impact value calculated from pathway topology analysis above 0.1 was filtered out as potential target pathway. In addition, fatty acid metabolism was also affected after 3d treatment because the levels of carnitine, several long chain carnitines and fatty acids were obviously changed, which were further analyzed below.

By comparing the 3d-treated group with the vehicle control group, 18 metabolites respective derived from glutathione metabolism, glycerophospholipid metabolism and fatty acid metabolism in HepG2 cells were highlighted, as shown in Fig. 5. Metabolites produced in glutathione metabolism contained reduced glutathione (GSH), L-cysteine, L-cysteinyl-glycine (L-Cys-Gly), and oxidized glutathione (GSSG). Glutathione metabolism plays a critical role in intracelluar antioxidant defense, redox regulation, and detoxification through the dynamic interaction of the GSH-GSSG redox couple in conjunction with various glutathione-dependent enzymes and transporter system [31,32]. GSH containing an important functional thiol group is a key intercellular antioxidant. It participates directly in the neutralization of free radicals and reactive oxygen

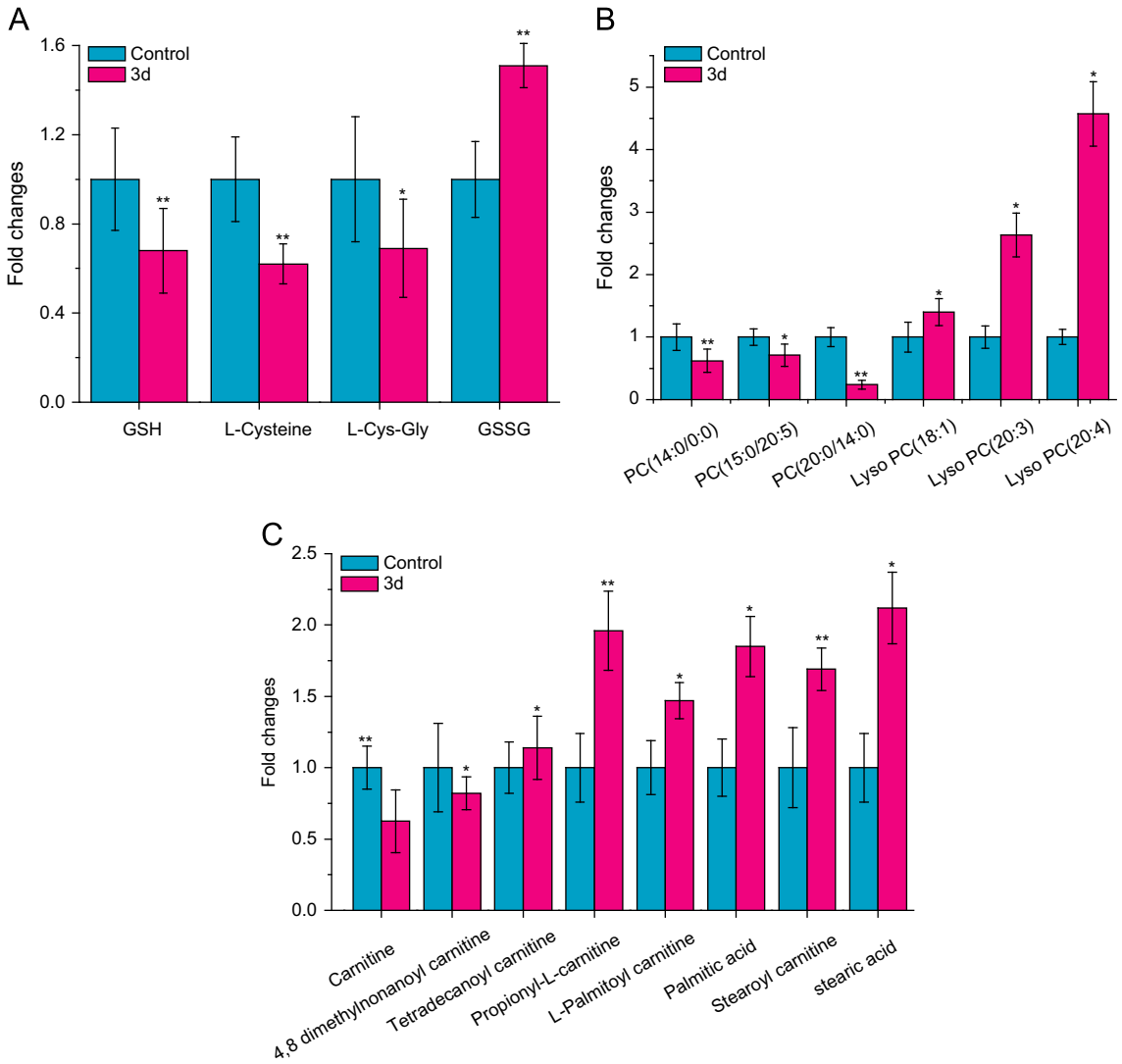

Fig. 5. The comparison of biomarker intensity between vehicle control and 3d-treated cells involved in (A) glutathione metabolism, (B) glycerophospholipid metabolism and (C) fatty acid metabolism ($n=8$), $^{*}p<0.05$ and $^{**}p<0.01$ compared with vehicle control.

compounds, as well as reducing oxidized or inactivate protein thiols in order to ensure their biological activities. Therefore, GSH is considered as an important indicator of oxidative stress [33]. As shown in Fig. 5A, GSH decreased by nearly 68% in 3d treated cells compared to the vehicle control (3d/control = 0.676 ± 0.189, $p < 0.05$). While the GSSG increased by nearly 150% (3d/control = 1.51 ± 0.149, $p < 0.05$). Furthermore, a significant decrease was noted in the levels of glutathione metabolites including cysteinylglycine and cysteine. These data suggested that celluar redox status was disrupted by 3d. The increased GSSG levels provided valuable information to support for the induction of oxidiative stress in 3d-treated cells. Furthermore, the significant decrease in the levels of glutathione metabloites suggested that there may be a reduced capacity to maintain intercellular redox homeostasis. It has been demonstrated that GSSG levels have close relationship with loss of mitochondrial integrity and caspase-activation [34]. The detrimental effects of oxidative stress induced by 3d might play a vital role in subsequent cellular antiproliferation to exhibit its antitumor activity.

We further investigated glycerophospholipid metabolism with a focus on lysophosphatidylcholines (LPCs) and phosphatidylcholines (PCs), as shown in Fig. 5B. Compared with the control group, three LPCs including LysoPC (18:1), LysoPC (20:3) and LysoPC (20:4) were increased by 1.40 times or more in 3d-treated cells. LPCs, a class of chemical compounds possessing a constant polar head, and fatty acyls of different chain lengths, position, and degrees of saturation, are products or metabolites of PCs. LPC level can be regarded as a clinical diagnostic indicator which reveals pathophysiological changes. It has been reported that LPCs can be formed during oxidation at the sn-2 fatty acid of PCs by ROS [35]. The results were consistent with the above observation of elevated oxidative stress level caused by 3d and further lead to lipid peroxidation. On the contrary, the levels of three PCs were significantly decreased ($p < 0.05$) in 3d-treated HepG2 cells, including two saturated fatty acid PCs [PC (14:0/0:0) and PC (20:0/4:0)] and one unsaturated fatty acid PC [PC (15:0/20:5)]. Because PCs are the main structural components of animal cell membranes, their decrease indicated the lesions of cell membrane induced by 3d [36].

Significant changes of 8 metabolites involved in fatty acid metabolism were also observed. After treated with 3d, intercellular carnitine and 4,8-dimethylnonanoylcarnitine were down-regulated, while tetradecanoylcarnitine, propionyl-L-carnitine, L-palmitoylcarnitine, palmitic acid, stearoylcarnitine and stearic acid were up-regulated (Fig. 5C). Carnitine is needed for the transport of long chain fatty acids and acyl coenzyme A derivatives across the inner mitochondrial membrane. Several researches have shown that carnitine possesses prominent protective effects against oxidative damage [37]. Carnitine not only participates in metabolism of ROS [38] but also plays a vital role in fatty acid metabolism [39,40]. The above results have shown that intercellular carnitine levels in 3d-treated group were significantly lower than the vehicle control, which indicated that carnitine might be expended to react with excessive ROS produced in 3d-treated HepG2 cells. The results were also consistent with the above observation of elevated oxidative stress level induced by 3d.

Table 2
Variation of 4 metabolites peak area involved in glutathione metabolism in three independent measurements expressed as RSD (%).

Metabolite	Glutathione	GSSG	L-Cys-Gly	L-Cysteine
Peak area	211.96	34.87	44.34	104.47
RSD (%)	7.90	5.89	8.88	7.64

3.4. Metabolites stability evaluation

Stability of metabolites is a major concern on the data accuracy of metabolomic studies due to the time-consuming of per sample analysis (about 10–30 min per sample). The stability of metabolites may be affected by enzyme activity, degradation of macromolecules to release metabolites, and inherent chemical lability. In order to evaluate the stability of metabolites, samples were reanalyzed three times with 12 h interval at 4 °C to mimic typical autosample storage. The metabolites involved in glutathione metabolism were mainly focused because of their inherent lability. The metabolites peak areas were compared with the initial values. As shown in Table 2, the relative standard deviation (RSD) in three independent measurements was less than 10%. These results indicated that the metabolites tested showed excellent stability in the experimental conditions.

3.5. 3d induces oxidative stress and mitochondria malfunction

The disturbance of glutathione metabolism, glycerophospholipid metabolism, fatty acid metabolism and the accumulation of GSSG have predicted the increased oxidative stress in 3d-treated HepG2

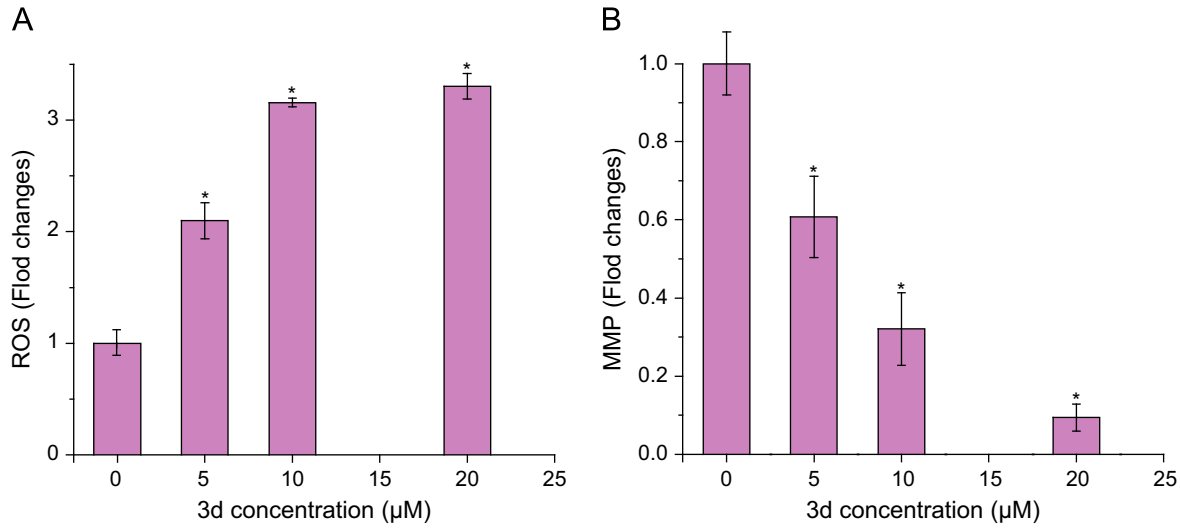

Fig. 6. The levels of ROS (A) and MMP (B) in HepG2 cells after treated with 3d (0–20 μM) for 24 h. Results are mean ± SD, $n = 3$, $^*p < 0.05$ compared with vehicle control.

cells. Intercellular ROS level and mitochondrial function were further characterized to prove the oxidative stress and cellular antiproliferation triggered by 3d. 3d-induced the generation of intercellular ROS was measured using a permeable fluorescence probe, DCFH-DA, which is oxidized to generate fluorescent DCF in the present of ROS [41]. After HepG2 cells were exposed to 0–20 μM 3d for 24 h, the fluorescence intensity of DCF was measured. As shown in Fig. 6A, the intercellular ROS levels were significantly increased with the increasing concentration of 3d ($p < 0.05$). ROS is very harmful to biological organism, such as attacking DNA to result in chain break, modification of carbohydrate parts, nitro bases, and amino acids in proteins, and causing injury to cell membrane by lipid peroxidation [42,43]. The remarkable increased LPCs indicated the lipid peroxidation induced by 3d which has been discussed above.

The mitochondria are one of the most important organelles for energy transduction within the cell to support cellular survival and a vulnerable intercellular target to ROS. Mitochondrial dysfunction contains a change in the MMP. In order to ensure whether the mitochondria were dysfunction, the changes in MMP were measured using a fluorescent dye Rh123. Rh123, a permeable cationic dye, preferentially partitions into mitochondria based on the highly negative MMP [44]. After HepG2 cells incubated with 0–20 μM 3d for 24 h, MMP was decreased drastically in a dose-dependent manner ($p < 0.05$) (Fig. 6B). When HepG2 cells were treated with 5, 10, and 20 μM of 3d, the fold changes of MMP to control cells were 0.607 ± 0.104, 0.320 ± 0.093, and 0.094 ± 0.035, respectively. The result demonstrated that the functions of mitochondria in HepG2 cells were indeed destroyed after treated with 3d. The mitochondrial dysfunction and the increased oxidative stress may in turn affect cellular metabolism, and finally lead to cellular antiproliferation.

4. Conclusion

In this study, a UPLC/Q-TOF MS based-metabolomics approach has been developed to investigate the metabolic profiling of HepG2 cells in response to 3d treatment in order to predict the hypothetic antitumor effect of 3d and its action mechanism. The metabolomics results indicated that intercellualr oxidative stress was increased after 3d treatment, and might induce the lesion of mitorchondria which were further verified by some biological experiments including the characterization of intercellular ROS and MMP after exposure to 3d. From the metabolomic and biological results, we propose that 3d-induced antiproliferation is associated with anomalous changes in redox homeostasis and mitochondria dysfunction. These findings enhance our understanding of the action mechanism of 3d antiproliferation and aid in its incorporation into further improvement.

Acknowledgments

This work was supported by the National Natural Science Foundation of China (Nos. 21172129 and 20935002), National Youth Science Foundation (No. 21305074), China Ministry of Science and Technology under Contract (No. 2012ZX09506001-010), International S&T Cooperation Program of China (No. 2011DFA30620), the National High Technology Research and Development Program of China (863 Program) (No. 2013AA092902), and Basic research projects in Shenzhen (No. JCYJ20120831165730898).

References

[1] J. Ma, Y.M. Yin, H.L. Liu, M.X. Xie, Curr. Org. Chem. 15 (2011) 2627–2640.
[2] E. Tripoli, M.L. Guardia, S. Giammanco, D.D. Majo, M. Giammanco, Food Chem. 104 (2007) 466–479.
[3] T. Cushnie, A.J. Lamb, Int. J. Antimicrob. Agents 38 (2011) 99–107.
[4] E.A. Rosa, B.C. Silva, F.M. Silva, C. Tanaka, R.M. Peralta, C. Oliveira, L. Kato, H.D. Ferreira, C.C. Silva, Rev. Bras. Farmacogn. 20 (2010) 484–488.
[5] S. Gómez-Alonso, V.J. Collins, D. Vauzour, A. Rodríguez-Mateos, G. Corona, J.P. Spencer, Food Chem. 130 (2012) 493–500.
[6] F. Jin, D. Gao, C. Zhang, F. Liu, B. Chu, Y. Chen, Y.Z. Chen, C. Tan, Y. Jiang, Bioorg. Med. Chem. 21 (2012) 824–831.
[7] F. Jin, N. Zhang, C. Tan, D. Gao, C. Zhang, F. Liu, Z. Chen, C. Gao, H. Liu, S. Li, Arch. Pharm. 345 (2012) 525–534.
[8] M. Tomosugi, Y. Sowa, S. Yasuda, R. Tanaka, H. te Riele, H. Ikawa, M. Koyama, T. Sakai, Cancer Sci. 103 (2012) 2139–2143.
[9] J.K. Nicholson, J.C. Lindon, E. Holmes, Xenobiotica 29 (1999) 1181–1189.
[10] H.-J. Choi, Y.-J. Yoon, Y.-K. Kwon, Y.-J. Lee, S. Chae, D. Hwang, G.-S. Hwang, T.-H. Kwon, J. Proteome Res. 11 (2012) 3816–3828.
[11] B.J. Blaise, J. Giacomotto, B. Elena, M.E. Dumas, P. Toulhoat, L. Ségalat, L. Emsley, Proc. Natl. Acad. Sci. USA 104 (2007) 19808–19812.
[12] M. Mayr, A. Zampetaki, A. Sidibe, U. Mayr, X. Yin, A.I. De Souza, Y.L. Chung, B. Madhu, P.H. Quax, Y. Hu, Circ. Res. 102 (2008) 1046–1056.
[13] T. Hisamatsu, S. Okamoto, M. Hashimoto, T. Muramatsu, A. Andou, M. Uo, M.T. Kitazume, K. Matsuoka, T. Yajima, N. Inoue, PLoS One 7 (2012) e31131.
[14] C. Ma, K. Bi, M. Zhang, D. Su, X. Fan, W. Ji, C. Wang, X. Chen, J. Ethnopharmacol. 130 (2010) 134–142.
[15] X. Lu, Z. Xiong, J. Li, S. Zheng, T. Huo, F. Li, Talanta 83 (2011) 700–708.
[16] N.P. Nørskov, M.S. Hedemann, P.K. Theil, K.E.B. Knudsen, Metabolomics (2013) 1–16.
[17] H.R. Cho, H. Wen, Y.J. Ryu, Y.J. An, H.C. Kim, W.K. Moon, M.H. Han, S. Park, S.H. Choi, Cancer Res. 72 (2012) 5179–5187.
[18] L. Zhang, X. Wang, J. Guo, Q. Xia, G. Zhao, H. Zhou, F. Xie, J. Agric. Food Chem. 61 (2013) 2597–2605.
[19] J.J. Kamphorst, J. Fan, W. Lu, E. White, J.D. Rabinowitz, Anal. Chem. 83 (2011) 9114–9122.
[20] A. Kiss, A.L. Jacquet, O. Paisse, M.M. Flament-Waton, J. de Ceaurriz, C. Bordes, J.Y. Gauvrit, P. Lanteri, C. Cren-Olive, Talanta 83 (2011) 1769–1773.
[21] C. Balderas, A. Villaseñor, A. García, F.J. Rupérez, E. Ibañez, J. Señorans, J. Guerrero-Fernández, I. González-Casado, R. Gracia-Bouthelier, C. Barbas, J. Pharm. Biomed. Anal. 53 (2010) 1298–1304.
[22] M.A. Lorenz, C.F. Burant, R.T. Kennedy, Anal. Chem. 83 (2011) 3406–3414.
[23] X. Xiao, Y. Hou, Y. Liu, H. Zhao, L. Dong, J. Du, Y. Wang, G. Bai, G. Luo, Talanta 107 (2013) 344–348.
[24] W. Cong, Q. Liang, L. Li, J. Shi, Q. Liu, Y. Feng, Y. Wang, G. Luo, Talanta 89 (2012) 91–98.
[25] S. Tiziani, A. Lodi, F.L. Khanim, M.R. Viant, C.M. Bunce, U.L. Günther, PLoS One 4 (2009) e4251.
[26] R. Devantier, B. Scheithauer, S.G. Villas-Bôas, S. Pedersen, L. Olsson, Biotechnol. Bioeng. 90 (2005) 703–714.
[27] P.K. Chrysanthopoulos, C.T. Goudar, M.I. Klapa, Metab. Eng. 12 (2010) 212–222.
[28] C. Servière, P. Fabry, Mech. Syst. Signal Proc. 19 (2005) 1293–1311.
[29] B. Zhou, J.F. Xiao, L. Tuli, H.W. Ressom, Mol. Biosyst. 8 (2012) 470–481.
[30] Y. Wu, L. Li, Anal. Chem. 84 (2012) 10723–10731.
[31] A. Pastore, G. Federici, E. Bertini, F. Piemonte, Clin. Chim. Acta 333 (2003) 19–39.
[32] H. Sies, Free Radical Biol. Med. 27 (1999) 916–921.
[33] M.A. Wilson, M.V. Johnston, G.W. Goldstein, M.E. Blue, Proc. Natl. Acad. Sci. U. S. A 97 (2000) 5540–5545.
[34] M.L. Circu, T.Yee Aw, Free Radic. Res. 42 (2008) 689–706.
[35] A. Catalá, Chem. Phys. Lipids 157 (2009) 1–11.
[36] M.M. Wright, A.G. Howe, V. Zaremberg, Biochem. Cell Biol. 82 (2004) 18–26.
[37] N. Tastekin, N. Aydogdu, D. Dokmeci, U. Usta, M. Birtane, H. Erbas, M. Ture, Pharmacol. Res. 56 (2007) 303–310.
[38] A.M. Weljie, R. Dowlatabadi, B.J. Miller, H.J. Vogel, F.R. Jirik, J. Proteome Res. 6 (2007) 3456–3464.
[39] C.R. Bruce, A.J. Hoy, N. Turner, M.J. Watt, T.L. Allen, K. Carpenter, G.J. Cooney, M.A. Febbraio, E.W. Kraegen, Diabetes 58 (2009) 550–558.
[40] F. Le Borgne, A. Ben Mohamed, M. Logerot, E. Garnier, J. Demarquoy, Biochem. Biophys. Res. Commun. 409 (2011) 699–704.
[41] A.P. Singh, S. Sarkar, M. Tripathi, S. Rajender, PLoS One 8 (2013) e54655.
[42] V. Lushchak, Biochemistry 66 (2001) 476–489.
[43] D. Wu, A.I. Cederbaum, Alcohol Res. Health 27 (2003) 277–284.
[44] J. Huang, C. Lv, M. Hu, G. Zhong, PLoS One 8 (2013) e58499.